EURODYN 2020
XI International Conference on Structural Dynamics
M. Papadrakakis, M. Fragiadakis, C. Papadimitriou (eds.)
Athens, Greece, 22âĂŞ-24 June 2020

EFFICIENT ESTIMATION OF THE SKEWNESS OF THE RESPONSE OF A WAVE-EXCITED OSCILLATOR

Margaux Geuzaine[1] **and Vincent Denoël**[2]

[1]Structural and Stochastic Dynamics, University of Liège, Belgium
Allée de la Découverte, Liège, B-4000
e-mail: {mgeuzaine,v.denoël}@uliege.be

[2] F.R.S-FNRS, National Fund for Scientific Research, Belgium
Rue d'Egmont, 8, B-1000 Bruxelles

Keywords: multiple timescales, spectral analysis, inertial loading, skewness, variance, wave loading.

Abstract. *The Multiple Timescale Spectral Analysis is a framework relying on the existence of well-separated timescales in the dynamic response of structures to generalize for higher-order statistics the famous background/resonant decomposition, widely applied by the wind engineering community to compute the variance of the response of SDOF structures or of each modal response of MDOF structures. This fast spectral analysis method mainly concerns the statistics of the response of onshore structures subjected to a buffeting wind loading whose characteristic frequency is typically lower than the natural frequencies of the structures concerned. By contrast, when dealing with wave-loaded floating offshore structures, the roles of the slow and fast timescales are likely to be interchanged and the method is extended further in this paper to compute rapidly the variances and the skewnesses of modal responses of such structures responding in the inertial regime as well, since these statistics are necessary to consider the influence of the non-Gaussianity of the loading.*

1 INTRODUCTION

The stochastic surge response of a floating structure is governed by a nonlinear differential equation. The nature of this equation is such that the basic input of the problem, the water particle velocity which is commonly assumed to be a Gaussian random process, results in a non Gaussian surge response [10]. As a consequence, the extreme value response might substantially differ from the results predicted with a Gaussian model, which would be based on the variance of the response only [11, 8]. A typical model developed in marine engineering is based on the cubic translation and the evaluation of higher statistical moments [16]. There are two approaches to the solution of this type of problem.

The first approach relies on the generation of samples of the problem input (the wave velocity) and the numerical solution of the problem based on appropriate time marching algorithms. In order to reduce the influence of the sampling and because of the coexistence of several timescales in the problem, namely the slow dynamics of the oscillator and the fast inertial wave loading, it is necessary to model very long signals with very short time steps. This makes this first method computationally intense although straightforward as to its practical implementation.[1],[7],[9]

The second approach consists in a spectral analysis and its higher order extensions [17, 10]. Although the strict equivalence between time and frequency domains vanishes as soon as the problem at hand features some nonlinearities, it is still possible to find relatively accurate estimates of the solution of the problem when the nonlinearities are limited [12]. The use of Volterra and Wiener series is one such approach [15, 13]. In a spectral approach, the variance of the response is obtained as a result of the integral of the power spectral density, while the third (and higher) moments are obtained by integration of the bispectrum (and higher spectra, respectively). Because of the existence of the several timescales in the response, the numerical integration of these spectra might be intense too. However, it is possible to take advantage of the specific form of the spectra and proceed to their Multiple Timescale Spectral Analysis [5]. This method consists in taking advantage of the known local shape of either factor of the spectra (either related to the load, either to the structural filter) and provide approximations of the integral. This method is known to be approximately two orders of magnitude (100 times) faster than a standard numerical integration. It founds its roots in the small correlation expansion [14] and has been being applied in wind engineering since the introduction of the famous background/resonant decomposition [2]. The Multiple Timescale Spectral Analysis generalizes several other similar approximations which provide a simple and rapid evaluation of the statistics of the structural response (covariance [3], third moment [4]) in linear or slightly nonlinear systems [6].

In this paper, the Multiple Timescale Spectral Analysis is specialized to the case of a single-degree-of-freedom system subject to a stochastic loading distributed over its resonant and inertial regimes, i.e. with a main loading frequency band above the natural frequency of the structure. This configuration is typical of the surge response of floating structures and would be typically tackled by means of a numerical integration of the spectra. Instead, we suggest to decompose the response, at second and third orders, as a sum of a resonant and an inertial components. Numerical validations demonstrate the accuracy of the proposed approximate, while being significantly faster.

2 FORMULATION OF THE PROBLEM

2.1 Governing equations

The force exerted by random waves on an oscillating point-like structure, which is undoubtedly small compared to the wavelength of waves, can be expressed according to the Morison equation by the sum of an inertial loading component

$$f_m(t) = k_m \dot{u}(t) \tag{1}$$

resulting from a linear transformation, as the overhead dot denotes partial differentiation in time t, of $u(t)$, the fluctuations of the water velocity around the constant current speed u_c, and a drag, or viscous, loading component

$$f_d(t) = k_d \left|u_c + u(t)\right| \left(u_c + u(t)\right) \tag{2}$$

depending on a nonlinear function of the water velocity, i.e. the sum of the current and the waves speeds. For the sake of simplicity in this short paper, the influence of the movement of the structure itself on the loading is considered as negligible. The coefficients k_m and k_d are related to geometric and hydrodynamic properties through:

$$k_m = c_m \rho_w v_w \quad \text{and} \quad k_d = c_d \rho_w a_w / 2 \tag{3}$$

where ρ_w is the water density, c_m is the inertia coefficient, c_d is the drag coefficient and a_w is the cross-sectional area of v_w, the volume of the submerged part of the structure.

The surge response of a single degree-of-freedom structure subjected to such a one-dimensional Morison-type force is therefore governed by the nonlinear second order differential equation

$$m\ddot{x}(t) + c\dot{x}(t) + kx(t) = f_m(t) + f_d(t) \tag{4}$$

where $x(t)$ is the displacement, k is the stiffness, c is the viscosity and m is the effective mass of the structure, i.e. the mass of the structure plus the added mass of fluid accelerating with the structure, as represented in Figure 1. Because of the memoryless nonlinearity included in the drag loading component, the response of the structure is expected to be non-Gaussian, even if the only input of the dynamical system, the random process $u(t)$, is supposed to be zero-mean, Gaussian, stationary and thus fully defined by its power spectral density $S_u(\omega)$.

The developments presented next are valid no matter the analytical or experimental definition selected for this power spectral density (PSD) but, in order to illustrate the results in a simple manner, the structure is assumed to be located at the still-water level in deep water. In this specific case, the application of the Linear Airy Wave Theory gives

$$S_u(\omega) = \omega^2 S_h(\omega) \tag{5}$$

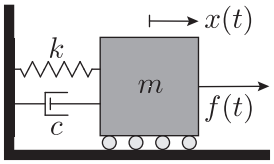

Figure 1: Typical single degree-of-freedom system

and it has been decided then to model the power spectral density $S_h(\omega)$ of the wave elevation process $h(t)$ by the two-sided Pierson-Moskovitz spectrum

$$S_h(\omega) = \frac{5}{32}\frac{\omega_h^4}{|\omega|^5}h_s^2 \mathrm{e}^{-\frac{5}{4}\left(\frac{\omega_h}{\omega}\right)^4} \tag{6}$$

with two parameters, h_s and ω_h, known as the significant wave height and the circular frequency corresponding to the peak of the spectrum of the wave elevation process. By cancelling the derivative of the PSD of the water velocity fluctuations, its own peak circular frequency, ω_u, is found to be equal to

$$\omega_u = \sqrt[4]{\frac{5}{3}}\omega_h \tag{7}$$

The power spectral densities employed in this paper are two-sided and their integration over the circular frequencies ω, from $-\infty$ to ∞, provides the variance of the associated process. Consequently, the variance of the water elevation process and the variance of the water velocity process are respectively given by

$$\sigma_h^2 = \left(\frac{h_s}{4}\right)^2 \quad \text{and} \quad \sigma_u^2 = \sqrt{\frac{3\pi}{4}}\omega_u^2\sigma_h^2 \tag{8}$$

2.2 Dimensionless formulation

A dimensionless formulation of this problem can be written by introducing a characteristic time t_r, a characteristic response x_r and a characteristic wave particle velocity u_r. Defining the dimensionless time $\tilde{t} = t/t_r$, the dimensionless displacement $\tilde{x}\left(\tilde{t}\right) = x\left[t\left(\tilde{t}\right)\right]/x_r$ and the dimensionless water velocity $\tilde{u}\left(\tilde{t}\right) = u\left[t\left(\tilde{t}\right)\right]/u_r$, Equation (4) becomes

$$\frac{m}{kt_r^2}\tilde{x}'' + \frac{c}{kt_r}\tilde{x}' + \tilde{x} = \frac{k_m u_r}{kx_r t_r}\tilde{u}' + \frac{k_d u_c^2}{kx_r}\left|1 + \frac{u_r}{u_c}\tilde{u}\right|\left(1 + \frac{u_r}{u_c}\tilde{u}\right) \tag{9}$$

after a divison by kx_r. The coefficient in front of the dimensionless drag loading component is set to unity by equalizing the characteristic elastic force kx_r to the force of the current $k_d u_c^2$. It is also chosen to define the reference time t_r as the inverse of $\omega_0 = \sqrt{k/m}$, the natural frequency of the system, in order to obtain a unitary coefficient in front of the highest order derivative. Lastly, the reference speed u_r is chosen as σ_u, the standard deviation of the water velocity process $u(t)$, and the presence of the turbulence intensity of waves, $\lambda_u = \sigma_u/u_c$, is hence revealed in the dimensionless formulation of the equation of motion

$$\tilde{x}'' + 2\xi_s\tilde{x}' + \tilde{x} = \kappa_u\lambda_u\tilde{u}' + |1 + \lambda_u\tilde{u}|\,(1 + \lambda_u\tilde{u}) \tag{10}$$

where the symbol $'$ denotes differentiation with respect to the new independent coordinate $\tilde{t}$. Besides,

$$\xi_s = \frac{c}{2m\omega_0} \quad \text{and} \quad \kappa_u = \frac{k_m\omega_0}{k_d u_c} \tag{11}$$

are respectively the structural damping ratio and the loading ratio. Similarly, Equation (5) is rewritten dimensionlessly as

$$S_{\tilde{u}}(\tilde{\omega}) = \sqrt{\frac{3}{\pi}}\frac{\varepsilon_u^2}{|\tilde{\omega}|^3}\mathrm{e}^{-\frac{3}{4}\left(\frac{\varepsilon_u}{\tilde{\omega}}\right)^4} \tag{12}$$

where $\tilde{\omega} = \omega t_r$ is the nondimensional circular frequency and $\varepsilon_u = \omega_u/\omega_0$ is the frequency ratio. The integration property of power spectral densities holds true for the nondimensional processes and can be applied to the rescaled water velocity process, $\tilde{u}(\tilde{t})$, to demonstrate that this input is now characterized by a unit variance, $\sigma^2_{\tilde{u}} = 1$, regardless the value of the frequency ratio ε_u. Interestingly enough, Equation (11) can be rearranged to introduce κ_c, the Keulegan-Carpenter number, that theoretically describes the relative importance of the drag loading component over the inertial loading component. It effectively plays this role in the equation of motion as it appears in the denominator of the loading ratio

$$\kappa_u = \frac{\varepsilon_u}{\kappa_c} \tag{13}$$

According to the Vashy-Buckingham theorem, the problem described in Equation (10) and Equation (12) is actually ruled by a set of four dimensionless numbers, $\{\xi_s, \lambda_u, \varepsilon_u, \kappa_u\}$. In wind engineering applications, where a very similar equation is encountered, these four parameters are typically all small and this property allows to simplify the governing equation. The inertial loading component is directly discarded and the absolute value is not needed anymore in the drag loading component since its argument is always positive. The expansion of the governing equation consequently yields

$$\tilde{x}'' + 2\xi_s\tilde{x}' + \tilde{x} = 1 + 2\lambda_u\tilde{u} + \lambda_u^2\tilde{u}^2 \tag{14}$$

in which the third term is at least one order of magnitude below the second because of the smallness of the turbulence intensity of wind, as detailed in [6]. In marine engineering applications, the structural damping ratio is usually still a small number, ranging between 10^{-3} and 10^{-1}, but the turbulence intensity of waves can reach values up to 2 or more. In addition, the loading ratio and the frequency ratio may take values above one, in the range $[10^0; 10^3]$, when wave-loaded structures are compliant in surge, as floating offshore wind turbines or floating bridges.

3 MULTIPLE TIMESCALE SPECTRAL ANALYSIS

Since the homogenous part of the dynamic system at hand (10) is linear, it is fully characterized by its frequency response function

$$H(\tilde{\omega}) = \frac{1}{1 - \tilde{\omega}^2 + 2i\xi\tilde{\omega}} \tag{15}$$

The PSD of the response thus takes the canonical form

$$S_{\tilde{x}}(\tilde{\omega}) = S_{\tilde{f}}(\tilde{\omega})\, K_s(\tilde{\omega}) \tag{16}$$

where the kernel function is, at second order,

$$K_s(\tilde{\omega}) \equiv |H(\tilde{\omega})|^2 = \frac{1}{\left(1 - \tilde{\omega}^2\right)^2 + 4\xi^2\tilde{\omega}^2}. \tag{17}$$

and, similarly, the bispectrum of the response is given by

$$B_{\tilde{x}}(\tilde{\omega}_1, \tilde{\omega}_2) = B_{\tilde{f}}(\tilde{\omega}_1, \tilde{\omega}_2)\, K_b(\tilde{\omega}_1, \tilde{\omega}_2) \tag{18}$$

where $B_{\tilde{f}}(\tilde{\omega}_1, \tilde{\omega}_2)$ represents the bispectrum of the loading. At third order, the kernel reads [4]

$$K_b(\tilde{\omega}_1, \tilde{\omega}_2) \equiv H(\tilde{\omega}_1)\, H(\tilde{\omega}_2)\, H(-\tilde{\omega}_1 - \tilde{\omega}_2) \tag{19}$$

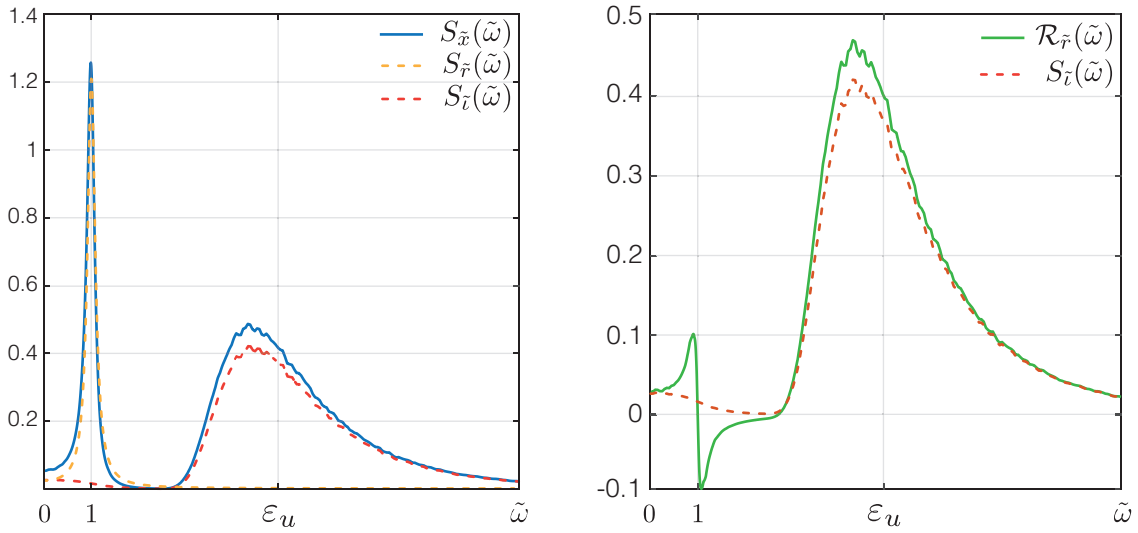

Figure 2: Typical shape of the PSD of the response (symmetrical, represented for $\tilde{\omega} \geq 0$) Numerical values: $\kappa_u = 10$; $\lambda_u = 1$; $\varepsilon_u = 5$ and $\xi = 10^{-1}$.

In a spectral approach, the statistical moments of the response are obtained by the (heavy) integration of the corresponding spectra, in particular

$$m_{2,\tilde{x}} = \int_{\mathbb{R}} S_{\tilde{x}}\left(\tilde{\omega}\right) \mathrm{d}\tilde{\omega} \qquad \text{and} \qquad m_{3,\tilde{x}} = \iint_{\mathbb{R}^2} B_{\tilde{x}}\left(\tilde{\omega}_1, \tilde{\omega}_2\right) \mathrm{d}\tilde{\omega}_1 \mathrm{d}\tilde{\omega}_2 \tag{20}$$

for the second and third moments. The Multiple Timescale Spectral Analysis aims at approximating these integrals with just a few operations [5], while providing at the same time a clear understanding of the different sources of contribution to the integral. Once statistical moments are determined, the skewness coefficient

$$\gamma_{\tilde{x}} = \frac{m_{3,\tilde{x}}}{m_{2,\tilde{x}}^{3/2}} \tag{21}$$

can be computed and used together with the peak factor model.

3.1 Second central moment of the response

As shown in Figure 2, when the frequency ratio ε_u is greater than one, the PSD of the response basically features:
- two resonant peaks having a width of ord (ξ) and being centered in $\tilde{\omega} = \pm 1$;
- two inertial peaks reaching their maximum value when $|\tilde{\omega}| = \text{ord}\left(\varepsilon_u\right)$ and spreading over the frequencies whose absolute value is above a given fraction ζ of the frequency ratio, $|\tilde{\omega}| > \zeta\varepsilon_u$;
- a flat background region in the vicinity of the origin.

As a first step, the introduction of the strained coordinates $\tilde{\omega} = \xi\tilde{\eta} \pm 1$, with $\tilde{\eta} = \text{ord}\left(1\right)$ at most, into Equation (16) allows to focus on the resonant peaks of the PSD of the response and the Taylor series expansion of the kernel function for small damping ratios yields

$$K_s\left(\xi\tilde{\eta} \pm 1\right) \simeq \frac{1}{4\xi^2}\left(\frac{1}{\left(\tilde{\eta}^2+1\right)} \mp \frac{\left(\tilde{\eta}^2+2\right)}{\left(\tilde{\eta}^2+1\right)^2}\xi\tilde{\eta} + \text{ord}\left(\xi^2\right)\right) \tag{22}$$

Likewise, the PSD of the loading is also expanded in Taylor series and reads

$$S_{\tilde{f}}\left(\xi\tilde{\eta}\pm 1\right) \;\simeq\; S_{\tilde{f}}\left(\pm 1\right) + S_{\tilde{f}}^{(1)}\left(\pm 1\right)\xi\tilde{\eta} + \text{ord}\left(\xi^2\right) \tag{23}$$

where the superscript (i) indicates the i-th derivative with respect to the dimensionless circular frequency $\tilde{\omega}$. While it seems reasonable to truncate Equation (22) at leading order on account that $\xi \ll 1$, it is necessary to check that the PSD of the loading is almost constant on the interval of interest, or more formally that

$$S_{\tilde{f}}^{(1)}\left(\pm 1\right) \;\leq\; \text{ord}\left(S_{\tilde{f}}\left(\pm 1\right)\right) \tag{24}$$

to be allowed to neglect higher order terms in Equation (23). If this condition is fulfilled, the PSD of the response is approximately equal to

$$S_{\tilde{r}}\left(\tilde{\omega}\right) \;=\; \frac{S_{\tilde{f}}\left(1\right)}{4\xi^2}\left(\frac{\xi^2}{\left(\left(\tilde{\omega}+1\right)^2+\xi^2\right)} + \frac{\xi^2}{\left(\left(\tilde{\omega}-1\right)^2+\xi^2\right)}\right) \tag{25}$$

in the regions spanned by the strained coordinates $\tilde{\omega} = \xi\tilde{\eta} \pm 1$, since the PSD of the loading is symmetric. This local approximation is represented by the yellow dashed line in Figure 2. The resonant component of the variance is eventually given by

$$m_{2,\tilde{r}} \;=\; \int_{\mathbb{R}} S_{\tilde{r}}\left(\tilde{\omega}\right)\mathrm{d}\tilde{\omega} = \frac{\pi}{2\xi}S_{\tilde{f}}\left(1\right). \tag{26}$$

Applying the procedure recommended in [5], the subtraction of $S_{\tilde{r}}\left(\tilde{\omega}\right)$ from the PSD of the response $S_{\tilde{x}}\left(\tilde{\omega}\right)$ provides a first residual with only two inertial peaks

$$\mathcal{R}_{\tilde{r}}\left(\tilde{\omega}\right) \;=\; S_{\tilde{x}}\left(\tilde{\omega}\right) - S_{\tilde{r}}\left(\tilde{\omega}\right) = S_{\tilde{f}}\left(\tilde{\omega}\right)\mathcal{K}_s\left(\tilde{\omega}\right) \tag{27}$$

in which

$$\mathcal{K}_s\left(\tilde{\omega}\right) \;=\; \left|H\left(\tilde{\omega}\right)\right|^2 - \frac{S_{\tilde{r}}\left(\tilde{\omega}\right)}{S_{\tilde{f}}\left(\tilde{\omega}\right)} \tag{28}$$

is the residual kernel function. A new coordinate stretching, $\tilde{\omega} = \left(\zeta\tilde{\eta}\pm 1\right)/\epsilon_u$ with $\epsilon_u = {}^1\!/_{\varepsilon_u} \ll 1$ and $\tilde{\eta} = \text{ord}\left(1\right)$ at most again, is then injected into Equation (27) to zoom on the inertial peaks. The Taylor series expansion of the residual kernel function for small values of ϵ_u yields

$$\mathcal{K}_s\left(\left(\zeta\tilde{\eta}\pm 1\right)/\epsilon_u\right) \;\simeq\; \frac{\epsilon_u^4}{\left(1\pm\zeta\tilde{\eta}\right)^4} - \frac{S_{\tilde{f}}\left(1\right)}{S_{\tilde{f}}\left(\left(\zeta\tilde{\eta}\pm 1\right)/\epsilon_u\right)}\frac{\epsilon_u^2}{\left(1\pm\zeta\tilde{\eta}\right)^2} \tag{29}$$

at leading order and the second term, coming from the approximations of the resonant peaks, can be discarded if

$$\frac{S_{\tilde{f}}\left(1\right)}{S_{\tilde{f}}\left(\left(\zeta\tilde{\eta}\pm 1\right)/\epsilon_u\right)} \;\leq\; \text{ord}\left(\epsilon_u^3\right) \tag{30}$$

in the interval of interest. However, even though the residual is correctly fitted by

$$S_{\tilde{\imath}}\left(\tilde{\omega}\right) \;=\; \frac{S_{\tilde{f}}\left(\tilde{\omega}\right)}{\tilde{\omega}^4} \tag{31}$$

in the regions spanned by the stretched coordinates $\tilde{\omega} = \xi\tilde{\eta} \pm 1$, this is not an appropriate local approximation, in the sense of the Multiple Timescale Spectral Analysis, because it is not always integrable near $\tilde{\omega} = 0$, regardless of the definition of the PSD of the loading. Considering, instead, the $(0, 4)$ Padé approximant

$$\mathcal{P}\,(0,4)\,[\mathcal{K}_s\,(\tilde{\omega})] = \frac{1}{1/\mathcal{K}_s\,(0) + \tilde{\omega}^4} \tag{32}$$

for the residual kernel, the local approximation

$$S_{\tilde{\imath}}\,(\tilde{\omega}) \;\; = \;\; \frac{S_{\tilde{f}}\,(\tilde{\omega})}{1/\mathcal{K}_s\,(0) + \tilde{\omega}^4} \tag{33}$$

of the residual is now integrable near $\tilde{\omega} = 0$ and matches the residual in the background region as well. The integrand is ultimately made totally independent from structural characteristics, such as the natural frequency of the system, by observing that $S_{\tilde{p}}\,(1) \simeq S_{\tilde{p}}\,(0)$, since $\varepsilon_u \gg 1$, and is represented by an orange dashed line in Figure 2. At the end, the mainly inertial, partly background, component of the variance of the response is given by

$$m_{2,\tilde{\imath}} \;\; = \;\; \int\limits_{\mathbb{R}} \frac{S_{\tilde{f}}\,(\tilde{\omega})}{2 + \tilde{\omega}^4} \mathrm{d}\tilde{\omega}. \tag{34}$$

and the variance of the response is approximated by the sum of the resonant and inertial contributions as

$$m_{2,\mathrm{mtsa}} \;\; = \;\; \frac{\pi}{2\xi} S_{\tilde{f}}\,(1) + \int\limits_{\mathbb{R}} \frac{S_{\tilde{f}}\,(\tilde{\omega})}{2 + \tilde{\omega}^4} \mathrm{d}\tilde{\omega}. \tag{35}$$

This approximation seems less advantageous, at first glance, than its equivalent background/resonant decomposition, since the inertial component is still expressed by means of an integral. Nevertheless, it is noticed that this integral only involves the loading and can be established, even maybe in closed-form, a priori, for a given PSD of loading.

3.2 Third central moment of the response

As shown in Figure 3, when the frequency ratio is greater than one, the bispectrum of the response exhibits essentially:
- six background bi-resonant peaks on an area of ord (ξ^2), centered in $(\pm 1, 0)$, $(\pm 1, 0)$ and $\pm\,(1, -1)$;
- six bi-resonant inertial peaks on an area of ord (ξ^2), centered in $\pm\,(1, -2)$, $\pm\,(2, -1)$ and $\pm\,(1, 1)$;
- six bi-background inertial triangular basins located between the background bi-resonant peaks and the bi-resonant inertial peaks;
- six resonant bi-inertial pairs of peaks, centered in $\pm\,(\varepsilon_u, 0)$, $\pm\,(0, \varepsilon_u)$ and $\pm\,(\varepsilon_u, -\varepsilon_u)$.

Focusing first on the region where $\tilde{\omega}_1$ and $\tilde{\omega}_2$ are both of ord (1), it appears quite clearly that the bispectrum of the response behaves locally as

$$B_{\tilde{r}}\,(\tilde{\omega}_1, \tilde{\omega}_2) \;\; = \;\; \Re\left[B_{\tilde{f}}\,(0,0)\right] K_b\,(\tilde{\omega}_1, \tilde{\omega}_2) \tag{36}$$

because the bispectrum of the loading is almost constant in this zone and its imaginary part is equal to zero. In addition, the third order kernel decreases fast enough along $\tilde{\omega}_1$ and $\tilde{\omega}_2$ for the

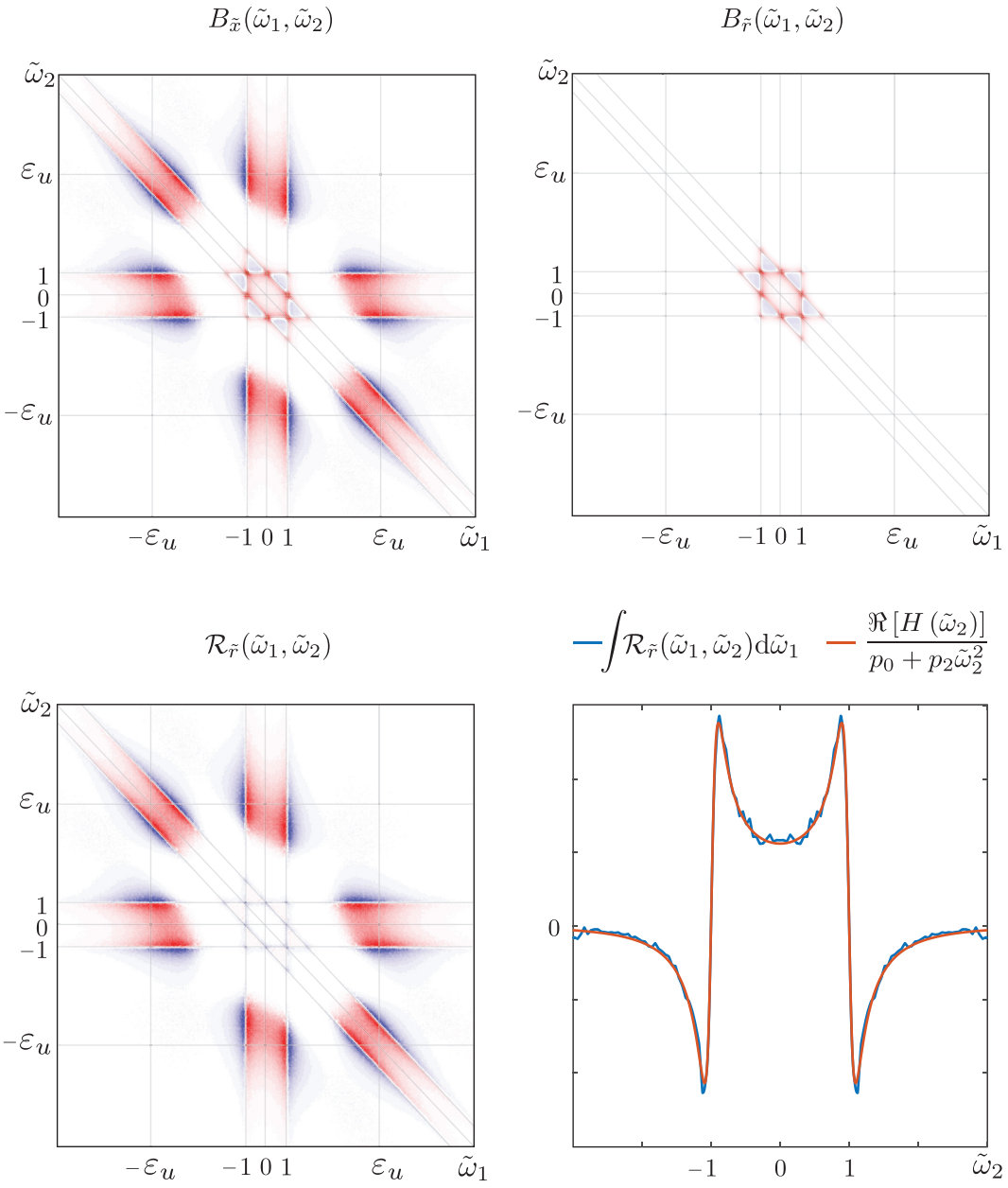

Figure 3: Typical shape of the bispectrum of the response $B_{\tilde{x}}(\tilde{\omega}_1, \tilde{\omega}_2)$. Numerical values: $\kappa_u = 10$; $\lambda_u = 1$; $\varepsilon_u = 5$ and $\xi = 10^{-1}$.

approximation presented in Equation (36) to be local and integrable, as required by the multiple timescale spectral analysis. Its double integration gives a simple and rapid estimation of the component of the third central moment of the response in the vicinity of the origin

$$m_{3,\tilde{o}} \quad = \quad \frac{8\pi^2}{3\left(1+8\xi^2\right)}\Re\left[B_{\tilde{f}}\left(0,0\right)\right] \tag{37}$$

which corresponds to the area under the six background bi-resonant peaks, the six bi-resonant inertial peaks and the six bi-background inertial triangular basins.

Then, the subtraction of $B_{\tilde{r}}\left(\tilde{\omega}_1,\tilde{\omega}_2\right)$ from the bispectrum of the response provides a first residual

$$\mathcal{R}_{\tilde{r}}\left(\tilde{\omega}_1,\tilde{\omega}_2\right) \quad = \quad \mathcal{B}_{\tilde{f}}\left(\tilde{\omega}_1,\tilde{\omega}_2\right) K_b\left(\tilde{\omega}_1,\tilde{\omega}_2\right) \tag{38}$$

where

$$\mathcal{B}_{\tilde{f}}\left(\tilde{\omega}_1,\tilde{\omega}_2\right) \quad = \quad B_{\tilde{f}}\left(\tilde{\omega}_1,\tilde{\omega}_2\right) - \Re\left[B_{\tilde{f}}\left(0,0\right)\right] \tag{39}$$

and a new coordinate stretching, $\tilde{\omega}_1 = \tilde{\eta}_1/\epsilon_u$ and $\tilde{\omega}_2 = \tilde{\eta}_2$ with $\tilde{\eta}_1$ and $\tilde{\eta}_2$ of ord$\left(1\right)$, is injected into Equation (38) in order to zoom on one of the resonant bi-inertial pair of peaks. The leading order term of the Taylor series expansion of the third order kernel for small values of ϵ_u corresponds to

$$K_b\left(\tilde{\omega}_1,\tilde{\omega}_2\right) \quad \simeq \quad K_s\left(\tilde{\omega}_1\right)\Re\left[H\left(\tilde{\omega}_2\right)\right] \tag{40}$$

where we recover the second order kernel and the real part of the frequency response function. Interestingly enough, each of those two distinguished functions depends on only one coordinate in the intervals of interest. In order to ensure the integrability of the local approximation near $\tilde{\omega}_1 = 0$ and $\tilde{\omega}_2 = \pm 1$, respectively, the second order kernel is approximated by a $\left(0,4\right)$ Padé approximant, similarly to what was done before with the inertial component of the PSD of the response,

$$\mathcal{P}\left(0,4\right)\left[K_s\left(\tilde{\omega}_1\right)\right] \quad = \quad \frac{1}{1+\tilde{\omega_1}^4} \tag{41}$$

and the real part of the frequency response function, on the contrary, cannot be simplified on account that the damping ratio is a small number. In addition, the variations of the bispectrum of the loading along $\tilde{\omega}_1$ and along $\tilde{\omega}_2$ have both to be taken into account. The first ones are indeed required to get a local approximation that resembles the residual while the second ones are needed to obtain a non-zero result for the resonant bi-inertial component of the third central moment of the response, since

$$\int_{\mathbb{R}} \Re\left[H\left(\tilde{\omega}_2\right)\right] \mathrm{d}\tilde{\omega}_2 \quad = \quad 0 \tag{42}$$

However, the number of points where the bispectrum has to be evaluated is drastically reduced by using a $\left(0,2\right)$ Padé approximant to fit correctly the integral of the residual along $\tilde{\omega}_1$ when $\tilde{\omega}_2$ is of ord$\left(1\right)$. It reads

$$\mathcal{P}\left(0,2\right)\left[\int_{\mathbb{R}} \frac{\mathcal{B}_{\tilde{f}}\left(\tilde{\omega}_1,\tilde{\omega}_2\right)}{1+\tilde{\omega_1}^4}\mathrm{d}\tilde{\omega}_1\right] \quad = \quad \frac{1}{p_0+p_2\tilde{\omega}_2^2} \tag{43}$$

in which

$$p_0 = \int_{\mathbb{R}} \frac{\mathcal{B}_{\tilde{f}}\left(\tilde{\omega}_1, 0\right)}{1+{\tilde{\omega}_1}^4} \mathrm{d}\tilde{\omega}_1 \quad \text{and} \quad p_2 = \int_{\mathbb{R}} \frac{\mathcal{B}^{(0,2)}_{\tilde{f}}\left(\tilde{\omega}_1, 0\right)}{1+{\tilde{\omega}_1}^4} \mathrm{d}\tilde{\omega}_1 \tag{44}$$

where the superscript (i,j) indicates the (i,j)-th derivative with respect to $\tilde{\omega}_1$ and $\tilde{\omega}_2$. It is worth to note that the Padé approximant is entirely independant from the structural characteristics again. The resonant bi-inertial component of the third central moment of the response is finally given by

$$m_{3,\tilde{\imath}} = \int_{\mathbb{R}} \frac{\Re\left[H\left(\tilde{\omega}_2\right)\right]}{p_0 + p_2 \tilde{\omega}_2^2} \mathrm{d}\tilde{\omega}_2$$

and the third moment of the response approximately corresponds to

$$m_{3,\text{mtsa}} \;=\; m_{3,\tilde{o}} + m_{3,\tilde{\imath}} \tag{45}$$

3.3 Numerical validation

The mathematical developments presented in Sections 3.1 and 3.2 are now validated by comparing the results obtained with the multiple timescale spectral analysis to the results coming from Monte Carlo simulations.

First, the PSD of the dimensionless water velocity fluctuations, $S_{\tilde{u}}\left(\tilde{\omega}\right)$, is computed according to Equation (12) for a given set of dimensionless numbers. A time-history of wave velocity fluctuations, $\tilde{u}\left(\tilde{t}\right)$, is then generated by computing the inverse Fourier transform of

$$U\left(\tilde{\omega}_i\right) \;=\; \sqrt{S_{\tilde{u}}\left(\tilde{\omega}_i\right) N \tilde{\omega}_s} \mathrm{e}^{\mathrm{j}\,\theta_i} \tag{46}$$

where $N = 10^8$ is the number of elements, $\tilde{\omega}_s = 20\ \varepsilon_u$ is the sampling circular frequency and θ_i is a phase angle randomly drawn from a uniform distribution in the interval $[0, 2\pi[$. At this point, it is already possible to check that the frequency content of the wave velocity signal is correctly represented by superimposing its PSD on the theoretical one. Figure 4 shows the very good agreement between them. Then, a loading sample is obtained by calculating

$$\tilde{f} \;=\; \kappa_u \lambda_u \tilde{u}' + \left|1 + \lambda_u \tilde{u}\right| \left(1 + \lambda_u \tilde{u}\right). \tag{47}$$

It is used differently in the time domain analysis and in the Multiple Timescale Spectral Analysis.

In time domain, the loading sample enters into the equation of motion which is hence solved numerically to obtain the evolution of the displacement of the structure in time, $\tilde{x}\left(\tilde{t}\right)$. To do so, the finite difference method with an explicit scheme has been chosen here but any other time marching algorithm would obviously provide almost exactly the same results. At the end, the second and third central moments of the response are respectively given by

$$m_{2,\tilde{x}} \;=\; \mathbb{E}\left[\left(\tilde{x}\left(\tilde{t}\right) - \mathbb{E}\left[\tilde{x}\left(\tilde{t}\right)\right]\right)^2\right] \tag{48}$$

$$m_{3,\tilde{x}} \;=\; \mathbb{E}\left[\left(\tilde{x}\left(\tilde{t}\right) - \mathbb{E}\left[\tilde{x}\left(\tilde{t}\right)\right]\right)^3\right] \tag{49}$$

where the operator $\mathbb{E}\left[.\right]$ stands for the mathematical expectation, computed over the samples.

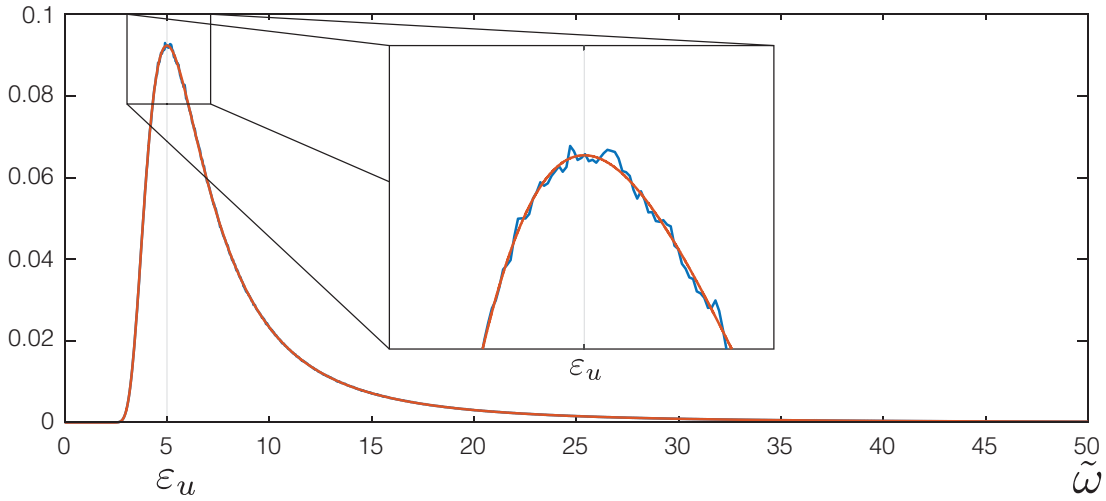

Figure 4: Typical shape of the power spectral density of the water velocity fluctuations.

In the spectral approach, we start by determining the power spectral density and the bispectrum associated to the loading sample. From there on, we just follow the steps detailed in Sections 3.1 and 3.2 to obtain the resonant and the inertial components of the second and third central moments of the response. Since we have kept the same set of dimensionless numbers throughout the whole paper, the local approximations and the first residual of the power spectral density and of the bispectrum of the response are respectively shown in Figure 2 and Figure 3.

The numerical results are summarized in Table 1 together with the computational time required in both cases. The second and third central moments of the response are computed much more rapidly with the Multiple Timescale Spectral Analysis and are very close to the references obtained with Monte Carlo simulations.

$S_{\tilde{f}}(1)$	$m_{2,\tilde{x}}$	$m_{2,\tilde{r}}$	$m_{2,\tilde{\imath}}$	$m_{2,\text{mtsa}}$	t_{time}	t_{mtsa}
0.05	3.58	0.76	2.60	3.36	5 s	0.1 s
$B_{\tilde{f}}(0,0)$	$m_{3,\tilde{x}}$	$m_{3,\tilde{o}}$	$m_{3,\tilde{\imath}}$	$m_{3,\text{mtsa}}$	$\gamma_{\tilde{x}}$	γ_{mtsa}
$8 \cdot 10^{-3}$	0.93	0.20	0.68	0.88	0.137	0.143

Table 1: Numerical values: $\kappa_u = 10$; $\lambda_u = 1$; $\varepsilon_u = 5$ and $\xi = 10^{-1}$

4 CONCLUSIONS

The background/resonant decomposition (which is widely applied in wind engineering) is a particular application of the Multiple Timescale Spectral Analysis where the natural frequency of the oscillator is larger than the frequency content of the loading. In this paper, we have specialized the concept to the companion problem, where the natural frequency of the oscillator is smaller than the characteristic frequency of the loading, as is typical in floating structures considered in marine engineering. Instead of the heavy numerical integration of the power spectral density and bispectrum of the structural response, the proposed methodology is able to determine the statistical moments of the response as a sum of two components. These two components correspond to a resonant contribution and an inertial contribution. The same decomposition is used for both the second and third orders. The resonant contribution takes a very similar shape as the well known existing approximations. Conversely to the companion problem though, the inertial contribution requires the evaluation of an integral, which is however

less cumbersome than in the formal numerical integration of the spectra since it involves the loading only.

The proposed methodology has been benchmarked against Monte Carlo simulations. It shows a significant CPU saving while offering a very competitive accuracy. It will certainly serve as a major cornerstone of a multi degree-of-freedom model, where the response of a structure in its modal basis will be computed as a linear combination of modal (single degree-of-freedom) responses.

ACKNOWLEDGEMENTS

The work of the first author is supported by a FRIA grant from the F.R.S-FNRS, the Belgian Fund for Scientific Research.

References

[1] R Adrezin, P Bar-Avi, and Haym Benaroya. Dynamic response of compliant offshore structures. *Journal of aerospace engineering*, 9(4):114–131, 1996.

[2] Alan Garnett Davenport. The application of statistical concepts to the wind loading of structures. *Proceedings of the Institution of Civil Engineers*, 19(4):449–472, 1961.

[3] Vincent Denoël. Estimation of modal correlation coefficients from background and resonant responses. *Structural Engineering and Mechanics: an International Journal*, 32(6): 725–740, 2009.

[4] Vincent Denoël. On the background and biresonant components of the random response of single degree-of-freedom systems under non-gaussian random loading. *Engineering structures*, 33(8):2271–2283, 2011.

[5] Vincent Denoël. Multiple timescale spectral analysis. *Probabilistic Engineering Mechanics*, 39:69–86, 2015.

[6] Vincent Denoël and Luigi Carassale. Response of an oscillator to a random quadratic velocity-feedback loading. *Journal of Wind Engineering and Industrial Aerodynamics*, 147:330–344, 2015.

[7] Ahmed A Elshafey, Mahmoud R Haddara, and H Marzouk. Dynamic response of offshore jacket structures under random loads. *Marine Structures*, 22(3):504–521, 2009.

[8] Mircea Grigoriu. Crossings of non-gaussian translation processes. *Journal of Engineering Mechanics*, 110(4):610–620, 1984.

[9] Zhiyu Jiang, Xiangqian Zhu, and Weifei Hu. Modeling and analysis of offshore floating wind turbines. In *Advanced Wind Turbine Technology*, pages 247–280. Springer, 2018.

[10] A Kareem and J Zhao. Analysis of non-gaussian surge response of tension leg platforms under wind loads. 1994.

[11] Dae Kun Kwon and Ahsan Kareem. Peak factors for non-gaussian load effects revisited. *Journal of Structural Engineering*, 137(12):1611–1619, 2011.

[12] YM Low. Frequency domain analysis of a tension leg platform with statistical linearization of the tendon restoring forces. *Marine Structures*, 22(3):480–503, 2009.

[13] Martin Schetzen. The volterra and wiener theories of nonlinear systems. 1980.

[14] Rouslan L Stratonovich. *Topics in the theory of random noise*, volume 2. CRC Press, 1967.

[15] SR Winterstein, TC Ude, and T Marthinsen. Volterra models of ocean structures: Extreme and fatigue reliability. *Journal of Engineering Mechanics*, 120(6):1369–1385, 1994.

[16] Steven R Winterstein and Tina Kashef. Moment-based load and response models with wind engineering applications. *J. Sol. Energy Eng.*, 122(3):122–128, 2000.

[17] Tokuo Yamamoto. Moored floating breakwater response to regular and irregular waves. *Applied Ocean Research*, 3(1):27–36, 1981.